Single-cell variability in a bacterial signalling network investigated by FRET

Istvan T. Kleijn

20th June 2013

Bachelor's Thesis

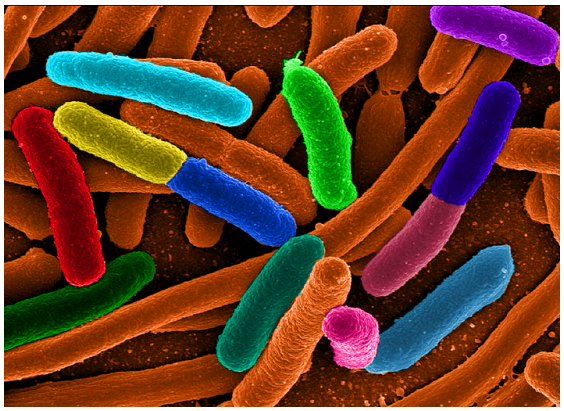

Department of Physics and Astronomy
Faculty of Science
Utrecht University

Supervisor:
dr. Thomas S. Shimizu
FOM Institute AMOLF

Universiteit Utrecht

FOM Institute AMOLF

Abstract

Chemotaxis is the ability of cells to sense their chemical environment and adjust their movement accordingly. In *Escherichia coli*, it has been extensively studied and has become a paradigm for signal transduction in biology. Despite its simplicity, it possesses many interesting network phenomena, most notably cooperative signal amplification and precise adaptation via a negative feedback. A fluorescence microscopy technique, Förster Resonance Energy Transfer (FRET), has proven to be a very effective experimental tool in characterizing the transfer functions of the signalling pathway in ensemble averaged measurements. While these functions provide a useful coarse-grained description in considering functional aspects, many open questions remain on the underlying molecular and cellular mechanisms. Therefore, we tailored the FRET technique to application at the single-cell level. We used this technique to characterise two different *E. coli* genotypes. First, in wild-type *E. coli* cells we measured the steady state kinase activity as well as the adaptation time scales to both repellent and attractant response. These parameters revealed earlier unnoticed differences between individual bacterial cells. Second, in *E. coli* cells lacking the genes necessary for adaptation we described the transfer functions of the receptor-ligand binding for individual cells. Counter-intuitively, we found that the parameters of the function describing this response varied significantly from cell to cell. This work forms a solid foundation for further investigations into cellular non-genetic variability in order to relate it to (i) heterogeneity of the motile behaviour of bacteria and (ii) differences in structural properties of cells.

Contents

1 Introduction

As George Orwell noted, some animals are more equal than others. Though they are not animals, the same adage goes for bacteria, albeit in a rather different fashion. Within one bacterial colony, inequality between cells is not due to any genetic differences, but to random processes. As bacteria are so small, their constitutions are very noisy. This causes variability in the chemical networks that govern a cell's life.

In this thesis, I will describe our work on investigating cell-to-cell variability in such a chemical signalling network. Before I will describe the research that has been part of my internship, I will give a general introduction to the topic. I will give a detailed description of the chemotaxis network in the bacterial species *Escherichia coli* and of Förster Resonance Energy Transfer, the fluorescence microscopy technique that we used. After this introduction, I will describe what work we have done in the past year. Firstly I shall explain the new experimental methods that we have developed. Then I will report on our findings when we apply these methods to the chemotaxis system.

1.1 Cellular signal processing

We humans spend most of our time awake doing the following: we observe our environment, we process these signals and then we act according to the outcome of this calculations. This same procedure holds for a single cell, but the way in which it is implemented obviously varies. Instead of in neural networks, the cellular signal processing takes place via chemical networks. One network usually consists of several proteins, which undergo conformational changes and chemical reactions such as phosphorylation and methylation (addition of PO_4- and CH_3-groups, respectively). These reactions are catalysed by the same proteins that make up the system. The efficiency of the catalysis depends on the conformational and chemical state of the enzyme (catalyst protein). We see that in such a chemical system, intricate positive and negative feedback loops may exist. Input to the system is usually given by a protein that has the ability to change under an outside influence. The output consists of one or more proteins that are sensed by some functional protein that can modify the cell or its environment, such as a molecular motor. We see that intricate systems have evolved, that can respond in very different ways to different stimuli.

1.1.1 Standard cell: *E. coli*

When studying properties of biological signalling networks, scientists have one model that stands out: *Escherichia coli* (*E. coli*). This bacterium is abundantly present in the intestines of humans and other mammals. It will grow under various circumstances, so it can be used in many different experiments. Furthermore, *E. coli* is not pathogenic. Also, it is relatively easy to modify the genome of bacteria (as opposed to more complex organisms). Therefore, these cells are ideal to study biological systems, as genetic modifications make it pos-

sible to investigate the individual components of the systems. For these reasons, *E. coli* has been developed into the "standard ruler" of cellular biology[6].

E. coli cells have a spherocylindrical shape, they are roughly 2 microns long and 0.5 micron wide. When they are grown in a rich medium, with lots of nutrients, they divide roughly once in 20 minutes. Most strains can swim: they can reach speeds of more than 20 microns per second, which is ten times their own length. At any given moment, about half of the cells dry weight is made up of proteins. There are more than 2 million protein molecules in one bacterium.

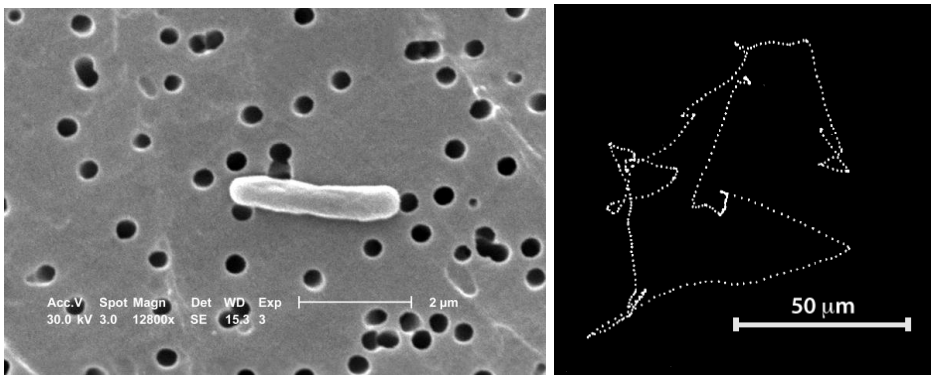

(a) (b)

Figure 1: a) Scanning electron microscopy image of an Escherichia coli bacterium, taken at a magnification of 12,800x. The scale bar is 2 micron. Image by CDC/Evangeline Sowers, Janice Carr. b) Map of the trajectory of an *E. coli* cell. Image by H.C. Berg, retrieved from `http://www.rowland.harvard.edu/labs/bacteria/index.php`, June 6, 2013.

1.1.2 *E. coli*'s strategy for finding food

One of the longest-studied biological systems is the one which bacteria (especially *E. coli*) use to find food and swim away from toxins: the so-called chemotaxis system. At first, this system was studied on a behavioural level. When one observes swimming bacteria under a microscope, one sees that they appear to follow a random walk. When studied more closely, one can see that the way they propel themselves is via long helicoidal flagella, about ten per organism, which the cells can rotate in two directions. When all flagella rotate in the same direction, they bundle together due to their helicoidality and the cell moves straightly. We call this a "run". When a flagellum starts spinning the other way, the cell gets stopped in its way due to friction. It will then rotationally diffuse. Hence, a cell gets a new orientation during this "tumble" event. When all flagella form again a bundle, the organism runs in a straight line, etcetera. This explains how bacteria exhibit a random walk.

The following question now raises itself: how can a bacterium use this apparently random mechanism to swim towards food? Nature has found an ingenious answer: a cell can extend the average length of the runs when it is swimming up a food gradient. The random walk is thus biased in the direction in which the food concentration is increasing.

The way a cell can influence the duration of the runs, is by varying the probability that a flagellum will spin in the correct direction . When the probability for a flagellum to spin in the correct direction is high, the runs will extend longer. Obviously, a cell wants to extend the runs when it is swimming in the direction where life is getting better. To do this, it has to be able to sense spatial gradients. A bacterium is too small to sense spatial gradients though. Typical chemical gradients are too small to vary significantly over the typical length of a cell. To overcome this problem, *E. coli* senses temporal gradients. As the swimming speed during a run is constant, this temporal gradient corresponds to a spatial gradient. This way, the bacterium may sense the direction in which conditions are improving, and act accordingly.

1.1.3 Cell-to-cell variability

The number of identical protein molecules in *E. coli* varies significantly between different protein species. In the system that governs chemotaxis in *E. coli*, the messenger protein CheY is quite abundant at $(8.2 \pm 0.3) \cdot 10^3$ copies per cell in rich medium. One bacterium has far fewer copies of the methylation enzyme CheR, only 140 ± 10[4]. We may expect quite some random noise in such small quantities. A simple model assumes that proteins are produced in some sort of Poisson process: the probability that a molecule will be produced in a given time interval is constant. Then the standard deviation of the number N of protein molecules of a given type will be $\sqrt{N}$. If $N \approx 100$, we get typical fluctuations of 10% of the protein number. This can have quite an impact on the system which the protein is part of.

This cell-to-cell variability may have certain benefits for the population. *E. coli* reproduces asexually: therefore all cells in a colony will have the same genome. This makes the colony vulnerable to environmental changes. When not all cells have the same phenotype though, some cells may have the possibility to adapt to the new circumstances.

From this we see that there is cell-to-cell variability between bacteria of the same colony. We now wonder how this variability can be seen on the molecular level. The research that is described in this thesis contributes to answering this question.

1.2 Chemotaxis protein network

We can split up the chemical network into two constituent parts: the receptor module and the adaptation module[12, 7]. The first one translates the concentration of attractant into something the flagellar motor uses to determine which way to rotate. The latter rescales the response, so that the system is being

saturated as little as possible. We will now describe the two modules in *E. coli*. Note that different species of bacteria may have slightly different versions of the chemotaxis network. For a graphical view of the system, see Figure 2.

1.2.1 Receptor module

E. coli senses its chemical environment in the following way. On the cell membrane, there are receptor proteins. These are specific for certain chemicals. For example, Tar receptors sense aspartate and Tsr receptors sense serine. These receptors are clustered together in trimers of dimers: nearly all receptors are coupled to another one, and most of those dimers assemble into trimers. The electrostatic interactions between the receptors makes them change shape when they are clustered. This causes cooperative behaviour: neighbouring receptors reinforce each other's stimuli.

The receptors change shape when they sense chemicals, and this influences the kinase CheA (via a scaffolding protein CheW). We denote a cell's kinase activity by $a \in [0, 1]$. This is the probability that a given kinase molecule in that cell will be active. It signifies the response of the bacterium to the given stimulus. When active, the kinase catalyses the phosphorylation of a messenger chemical, CheY. This moves the equilibrium of the following reaction to the right:

$$CheY + P \rightleftharpoons CheYP \tag{1}$$

The key output chemical of the signalling network is CheYP, the phosphorylated form of CheY. The lower the concentration of CheYP is, the more the motors will bundle the flagella, which elongates the runs.

The effects of the kinase are countered by the enzyme CheZ. This protein catalyses the dephosphorylation of CheY, so it moves the equilibrium of equation 1 to the left.

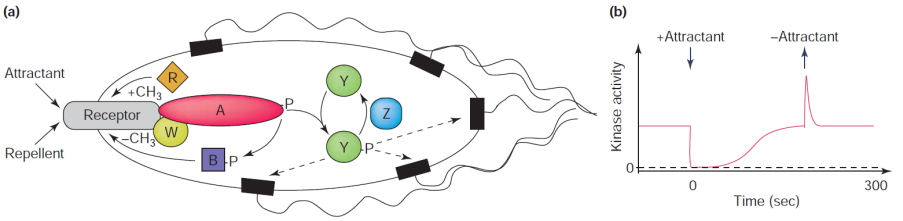

Figure 2: a) Overview of the chemotaxis signalling network in *E. coli*. b) Typical response of the system to an addition of attractant and subsequent removal. Image taken from [8].

1.2.2 Adaptation module

The chemotaxis system has another important feature: the ability to adapt to its environment. The proteins responsible for this are CheR and CheB. CheR adds methyl groups to the receptors, CheB removes them. One receptor has four methylation sites. When a receptor has more methyl groups attached, it will need more attractant to make the kinase turn active.

As illustrated in figure 2b), the adaptation to the addition of attractant (caused by methylation) goes slower than the adaptation to the removal of attractant. Both types of adaptation occur much slower than the time scale of the receptor module, in which the kinase activity reacts to the step changes in stimulus.

1.2.3 Dose-response curves

A standard way of looking at the signalling network, is by acquiring a dose-response curve. To get such a curve, one applies varying amounts of stimulus (usually attractant) and investigates the response of the network as compared to a baseline in buffer. This response is characterized by the value of a, which we recall to be the probability of the kinase to be active. The kinase activity depends on ligand concentration $[L]$ and the state of methylation m.

When we assume a two-state model, this probability will be given by[12]

$$a = G([L], m) = \frac{1}{1 + e^{f([L],m)}} \tag{2}$$

where $f([L], m)$ is the difference in (dimensionless) free energy between the active and inactive state.

Now the receptors are clustered in the membrane, and their interactions have the effect of amplifying the response. This is called cooperativity. A Monod-Wyman-Changeux model[5] can be used to describe the effects of cooperativity. This assumes that N identical receptors form a cluster. Different cluster do not interact with each other. Using this model, the free energy difference can be written as

$$f([L], m) = N\left(f_m(m) + f_L([L])\right) = N\left(f_m(m) + \ln\frac{K_I + [L]}{K_A + [L]} - \ln C\right)$$

so the free energy can be separated in a part f_m that only depends on the methylation and a part f_L that only depends on the ligand concentration. Here K_I and K_A are the dissociation constants[1] of the ligand for the inactive and active state, respectively, and $C = \frac{K_I}{K_A} \ll 1$. In practice, we apply ligand concentrations which are too small to occupy active receptors but large enough to occupy all inactive receptors, so $K_I \ll [L] \ll K_A$. The free energy then simplifies to

[1] The dissociation constant signifies the concentration of ligand at which half of the receptors are occupied by a ligand molecule.

$$f([L], m) = N\left(f_m(m) + \ln\left(\frac{[L]}{K_I}\right)\right)$$

which we can insert in equation 2 to obtain

$$a = \frac{\left(K_I e^{-f_m(m)}\right)^N}{\left(K_I e^{-f_m(m)}\right)^N + [L]^N}$$

According to the model, the kinase activity as a function of applied steps in the ligand concentration $[L]$ is thus given by a Hill curve:

$$a([L]) = \frac{k_{\frac{1}{2}}^H}{[L]^H + k_{\frac{1}{2}}^H} \tag{3}$$

which is a sigmoid curve that saturates to 1 for $[L]$ small and to 0 when $[L]$ big. Here $k_{\frac{1}{2}}$ is the ligand concentration where the activity is at half its maximum. The parameter H is called the Hill coefficient; it signifies the steepness of the curve.

Dose-response curves are thus a way to probe the model, the parameters $k_{\frac{1}{2}}$ and H relate to the model in the following way:

$$\begin{aligned} k_{\frac{1}{2}} &= K_I e^{-f_m(m)} \\ H &= N \end{aligned} \tag{4}$$

1.3 Förster Resonance Energy Transfer

To get information on the network level, we make use of a fluorescence technique called Förster Resonance Energy Transfer (FRET). This technique enables us to get quantitative data on the kinase activity as a function of the applied stimulus. The technique was described thoroughly in[10].

1.3.1 Fluorescence

In biophysics, many experimental techniques make use of fluorescence. This means that we excite the ground state of a suitable molecule, called a fluorophore, with a photon. The excited state then first relaxes non-radiatively. After this, it relaxes to the ground state by emitting a photon. This emitted photon has a lower energy than the accepted one. The principle is illustrated in figure 3.

Several proteins have been discovered that can be used as fluorophores. When one studies biological organisms, these fluorescent proteins can be encoded onto the DNA of the studied organism. A useful application is, to join the fluorescent protein to another, biologically interesting one. One can then follow the fluorescence to discover something about the protein that the fluorophore is joined to.

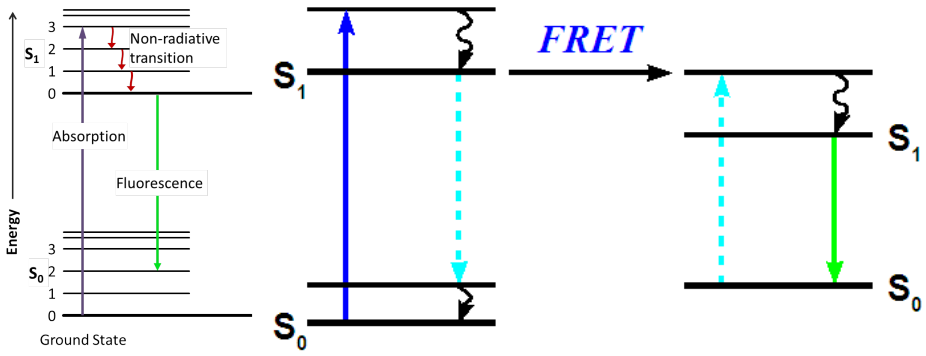

Figure 3: Illustration of energy transfer in generic fluorescence(left) and in FRET (right).

1.3.2 Principle of FRET

The fluorescence technique that we use is called Förster Resonance Energy Transfer (FRET). It exploits the fact that energy can be transferred non-radiatively from one fluorophore to another. The way FRET works, is as follows. One needs two suitable fluorescent proteins: a donor and an acceptor protein. The donor D is excited at a higher photon energy than the acceptor A. When both proteins are close enough together, energy may be transferred upon excitation of D from D to A. One then sees fluorescence at a lower frequency than without this process. The principle is illustrated in figure 3.

The efficiency of FRET η_{FRET} depends strongly on the distance r between the two proteins, notably in the following way:

$$\eta_{FRET}(r) = \frac{R^6}{r^6 + R^6}$$

where R is a fixed parameter (the Förster radius), which depends on the particular proteins. It is typically about 5 nm.

From this equation we see, that FRET will only occur when the donor and acceptor are very close together. We can exploit this property when we want to look at chemical reactions, by ensuring that we see more FRET when a certain reaction occurs.

We genetically engineer the bacteria in the following way. We co-express a donor fluorescent protein with CheZ and an acceptor fluorophore with CheY.

This means, that the cells will produce CheZ proteins with the donor protein attached at one end of the amino acid sequence, and likewise for CheY. Obviously, we have to be careful when selecting the fluorescent proteins: we want that the bacteria's enzymes remain functional.

When now CheZ and CheY form a complex, the donor and acceptor will be close together. This induces FRET. Hence, we see FRET when CheZ is dephosphorylating CheYP. But in equilibrium, this goes at the same rate as the phosphorylation of CheY by CheA, and this is precisely the kinase activity.

1.3.3 FRET is proportional to kinase activity

When D_0 is the intensity of our donor in the absence of FRET, and ΔD the change in intensity, we can define our FRET signal as

$$\frac{\Delta D}{D_0} = \eta_{FRET} \frac{[CheYP \cdot CheZ]}{[CheZ]_{tot}}$$

where $[CheYP \cdot CheZ]$ is the concentration of CheZ that forms a complex with CheYP and $[CheZ]_{tot}$is the total concentration of CheZ in the cell, including both bound and unbound molecules. As η_{FRET} is a constant that only depends on the construct and $[CheZ]_{tot}$ is constant for each cell, we find

$$\frac{\Delta D}{D_0} \propto [CheYP \cdot CheZ] \propto a \tag{5}$$

1.3.4 Ratio of red to green signal

In practice, it is rather hard to monitor the intensity of the donor protein. The noise in the signal is very high and we also have the problem, that the fluorophores are destroyed by the laser light (see next section). To reduce the noise, we can look at the ratio of intensities in the acceptor and the donor channel, in the following way.

Define r as the ratio of intensities from acceptor and donor, so $r = \frac{A}{D}$. When we observe FRET, the acceptor and donor intensities change from their baseline levels A_0 and D_0 by amounts ΔA and ΔD, respectively. As ΔA is positive when ΔD is negative (energy is transferred from donor to acceptor), and the amount of transferred energy is constant for a given set-up, we can define the positive constant $\alpha = -\frac{\Delta A}{\Delta D}$. Define $r_0 = \frac{A_0}{D_0}$. Now the change in the ratio will be $\Delta r = \frac{A_0 + \Delta A}{D_0 + \Delta D} - r_0$. We can now rewrite the FRET signal as

$$\frac{\Delta D}{D_0} = -\frac{\Delta r}{\alpha + r_0 + \Delta r} \tag{6}$$

We therefore see that the FRET signal will be proportional to the change in the ratio of donor and acceptor intensities, when $\alpha + r_0$ is much greater than Δr. This ratio is more robust than the change in donor intensity, because some sources of noise will work equally on the donor and acceptor. Because the FRET signal is proportional to the kinase activity, we now have a robust way of measuring the kinase activity a.

1.3.5 Application of FRET to *E. coli* chemotaxis

FRET techniques have been successfully used to probe *E. coli*'s chemotaxis network on a population level. In figure 4, taken from[10], we see an acquired dose-response curve on a population of cells that did not express CheR and CheB, so they did not adapt to their environment. The FRET pair used was CFP/YFP.

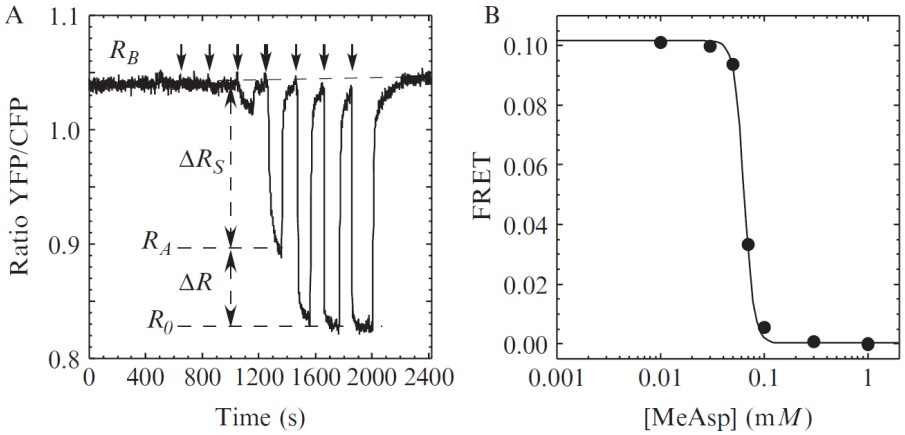

Figure 4: A) Plot of the ratio between acceptor and donor signal as a function of time, measured in a population of non-adapting cells. At the arrows, concentrations of the amino acid methylaspartate (MeAsp) were added and removed after some time . B) Dose-response curve calculated from the ratio signal in A).

It is of course also possible to apply FRET to adapting cells. A way to examine the adaptation dynamics is the following. When we give a saturating amount of attractant to the bacteria, the kinase activity will drop to zero. Then CheR will start methylating the receptor, but the system will remain saturated for some time. At some time, the methylation will take the system out of saturation, and the kinase activity will climb back to a new steady-state level. This level does not need to be the same as the initial steady-state activity, but for populations of *E. coli* in MeAsp, it comes quite close. Now we can remove the attractant. This will induce a repellent response: the kinase activity will increase rapidly. However, a concentration that saturates the attractant response does not necessarily saturate the removal response. When we choose a high enough concentration of attractant, the system will get saturated in both cases. When the kinase activity is at its maximum, CheB will demethylate the receptors and a will fall down again to the steady-state level. As the methylation and demethylation is governed by different enzymes, it is to be expected that adaptation to attractant and repellent will be different from one another. Indeed this is the case: the bacteria adapt much faster to the removal response. On a population level, the kinase activity during this kind of experiments looks like what is shown in figure 5.

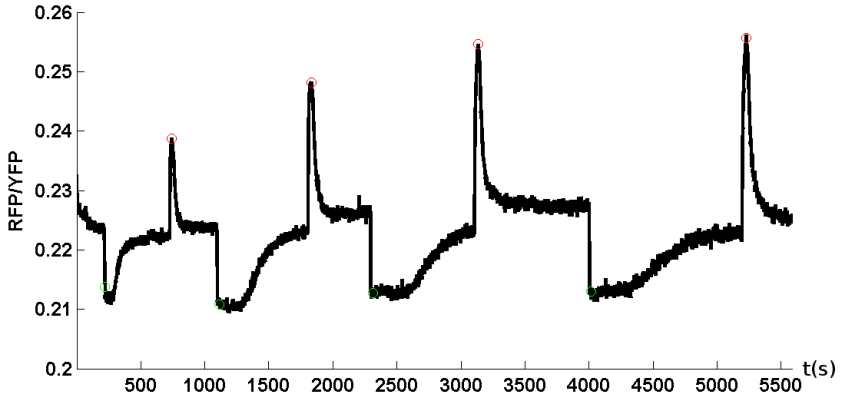

Figure 5: Ratio of red to green intensities in a population experiment as a function of time in seconds. Four different concentrations of MeAsp were added and subsequently removed, namely 0.01, 0.1, 0.5 and 1 mM.

2 Methods

Now I will go on to describe our recent work on the application of FRET at a single-cell level. Firstly, I will discuss our work on the experimental set-up. Then I will describe what we have measured with this assay.

To apply single-cell FRET, one works with very small numbers. As noted, a typical *E. coli* cell contains only several thousand copies of CheY and CheZ. This means that each cell has only this small amount of fluorescent proteins. To get enough signal for each cell, we make use of a very sensitive camera, capable of measuring almost single photons. Additionally, we use laser light with high excitation intensity. Problematically, blue light has a toxic effect on bacteria[11]. This problem has induced us to use YFP-mRFP as our FRET pair, instead of CFP-YFP which is used for population-FRET[1]. Because of this, we can use laser light with a higher wavelength. This reduces the destructive effects of the laser.

We ended up using a 515 nm laser. It had a total illumination power of 15 mW. The bundle had a Gaussian shape, the full width at half maximum was 40 microns. Therefore, the maximal intensity was $5.5 \cdot 10^8$ W m^{-2}.

2.1 Photobleaching and baseline correction

When we acquire FRET measurements on single cells, we observe a significant drift in the signal, as seen in figure 7. This drift makes it hard to compare the kinase activities over an extended period of time. We therefore want to find a way to correct for this drift and find a constant baseline against which we can compare the responses.

If we look at the measured light intensities, we see that these fall off, approximately exponentially. The way we understand this, is the following. When a fluorescent protein molecule is being excited by light, it enters an excited state. The chemistry of this excited state may very well be different than that of the ground state. For instance, the fluorophore may be completely ionized by the laser light. Hence, when a fluorophore is being excited, there is a chance that it degrades by some chemical reaction. We call this effect photobleaching. This effect is not completely understood. Furthermore, it varies between different fluorophores.

When at any time there is a constant probability that a fluorophore will bleach, we are dealing with a Poisson process. This would mean that the signal would decrease exponentially over the measurement length. As there might be several of these processes going on at the same time, the picture gets more complicated. In practice, the decreasing signal is well fitted by a double exponential function $I_f(t) = A_1 \exp(-\lambda_1 t) + A_2 \exp(-\lambda_2 t) + B$. An example can be seen in figure 6.

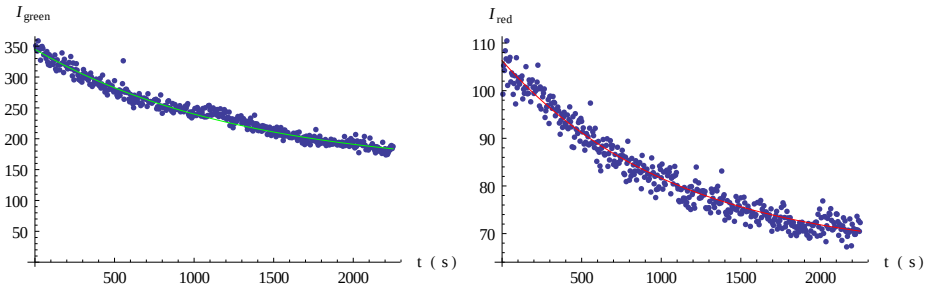

(a) Fit of baseline intensity in green channel. (b) Fit of baseline intensity in red channel.

Figure 6: Plots showing the measured intensities in photon units and the fitted baseline for both light channels in one cell.

2.1.1 Autofluorescence

One thing to be careful of, is the fluorescence that we may observe due to fluorescence of proteins different from our FRET pair, that may be around in the cell. When we take the ratio of red to green light, we assume that all the light we observe is actually coming from our FRET pair. It appears that we may neglect this for the following reason.

In a strain of cells that did not express fluorophores, we measured the autofluorescence directly. We found this to be only of the order of 1% of the signal observed in cells with fluorophores. Additionally, we could still see FRET responses in the cells that did express the FRET pair, even when the fluorophores were bleached until the point where the intensities were approximately constant. Hence, we neglect the effect of autofluorescence.

2.1.2 Fitting and rescaling

Our scheme to deal with photobleaching is the following. We fit a double exponential function $I_f(t)$ to both the red and the green intensity[2]. We then take the difference of the measured values for the intensity I_m and I_f at all time points t. Then we rescale everything by adding up $I_f(0)$ to all data points. The formula for the rescaled intensity I_r becomes

$$I_r(t) = I_m(t) - I_f(t) + I_f(0)$$

This procedure ensures that the baseline ratio is constant for all cells. In figure 7, we see the result of this rescaling procedure.

[2]We use only those data points for which the chemical stimulus was the same, as defined by our specific protocol for that day.

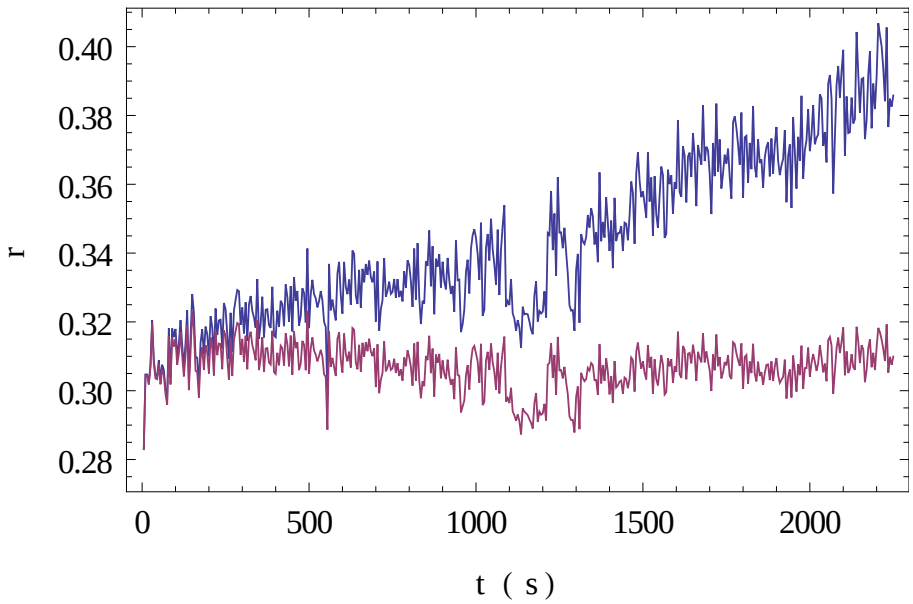

Figure 7: Time series of the ratio of red to green light for the same cell as used for figure 6. In blue we see the original ratio, in red we have the bleaching-corrected one.

2.2 Phototoxicity

As we have seen, laser light has the ability to induce chemical reactions that involve proteins (such as the fluorophores that we use). When these chemical reactions happen inside the cells, we may be disturbing the chemotaxis network. In this section, I will explain the experiment that we have done to characterise how much our measurement strategy perturbs the system.

We have studied this issue, by measuring the kinase activity at the same chemical stimulus but with various laser powers. We performed two different experiments. In the first, we changed the intensity of the excitation light directly. In the second, we varied the length of the time interval between the laser pulses.

Because we need to decrease the laser power, our signal quality decreases. Therefore we cannot measure the responses of single cells. These measurements were thus performed on populations of cells.

2.2.1 Influence of laser power

The first way that we changed the laser intensity was by putting different neutral density filters (ND's) in the light path, between the laser and the cells. As our reference, we used two filters, which let through only 9.2% of the laser light. This was the lowest laser power used. The highest power we investigated was

our usual one (15 mW of total illumination power). We also checked a medium power, for which we used only one of the two filters. This transmitted 25% of the light. We calibrated the filters using a photo-diode and oscilloscope, which lead to the stated numbers.

An important feature of non-adapting cells is the following. Their steady-state kinase activity in buffer is close to 1. This means that it is not possible to measure repellent responses when the cells are exposed to MotM only, as a repellent response would mean an increase in kinase activity. Therefore, we used a baseline stimulus of 0.05 mM L-serine in MotM. This way, both attractant and repellent responses could be seen.

To look at the range of possible kinase activities, we gave two stimuli: first we removed the 0.05 mM L-serine, so the stimulus was just MotM. Then we applied a saturating amount of L-serine: 0.5 mM. We repeated this procedure five times: first for low power, then for high, then low, then medium and then low power again. The acquired time series is shown in figure 8. This data was acquired on the same population of cells, only changing the filters in between. The signal is not corrected for bleaching.

At the first run at low power, we see that the kinase activity first goes up (to 1), this is the response to the removal of the 0.05 mM. Then it drops down (to 0) when we apply the saturating concentration of 0.5 mM. The other runs show an extra drop in the kinase activity before the removal response. This is caused by the small amount of saturating stimulus which was still in the tubing.

An interesting feature of this test is the following. We see that the baseline ratio depends on the applied laser power. This means that the amount of FRET we observe does not depend linearly on the intensity of the light that we apply. There are several contributions, among others the background varies with the intensity and we are dealing with leakage from the green to the red channel. It is thus difficult to relate the ratio as measured at different powers directly to changes in the kinase activity. For each laser power separately, we can look at how the kinase activity changes due to chemical stimuli.

We can qualitatively see from the picture, that the response of the cells to the chemical stimulus does not appear to vary significantly when we change the laser power. This has been made quantitative in the following way. For each laser power, we did the following. To correct the ratio for bleaching, we fitted a straight line to the ratio, using the points where 0.05 mM serine was applied. We then calculated the difference from this baseline for each point. We took the average of this difference both in buffer and in saturating concentration. The result of this is plotted in figure 9a. As can be seen, the overall size of the responses is indeed very similar. Application of high laser power seems to permanently lower the amplitude of the response somewhat, but this effect is not so large as to invalidate the usage of this high power.

Furthermore, we investigated if the laser power affects the chemotaxis system as follows. We calculated the fraction $\frac{\Delta r_+}{\Delta r_-}$, where Δr_+ is the change in ratio upon going from 0.05 mM to 0.5 mM serine, and Δr_- is the change in ratio when removing the 0.05 mM stimulus. As can be seen in figure 9b, the system

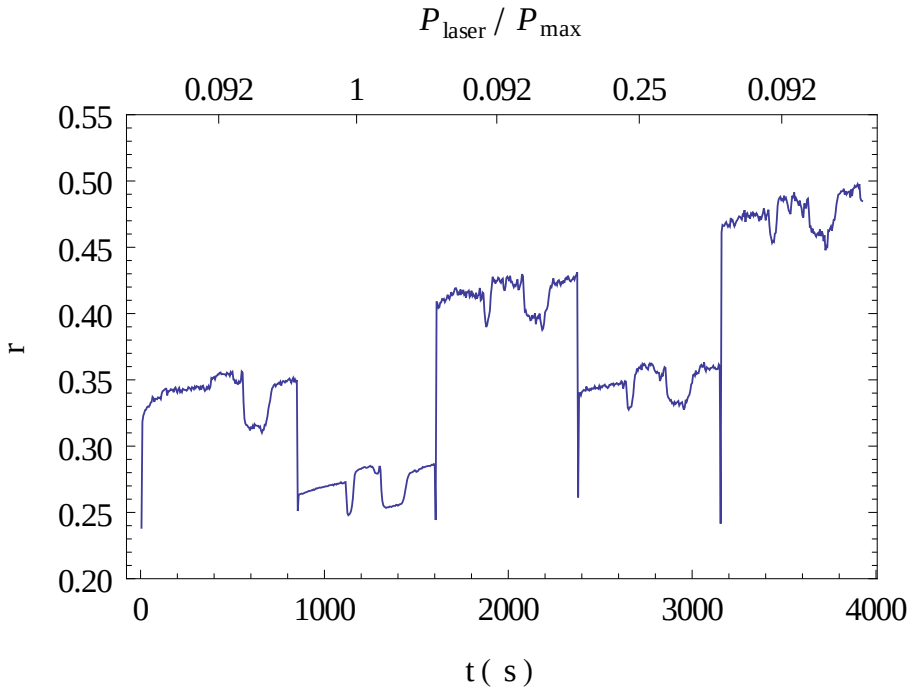

Figure 8: Plot of the FRET ratio in the experiment where we varied the laser power directly. No background correction was applied. The large discontinuities arise when we switch between the different laser powers. The smaller features are caused by the cellular response to chemical stimuli.

might be affected by the high laser power, as this fraction is higher with higher laser power. However, it is highly non-linear, as the aberration is far greater with medium power than with high power. Also, the high power does not seem to have a permanent harmful effect on the cells, as the calculated fraction at low power restores to its original value after application of high power.

From the previous discussion, we conclude that it is safe to use this high a laser power.

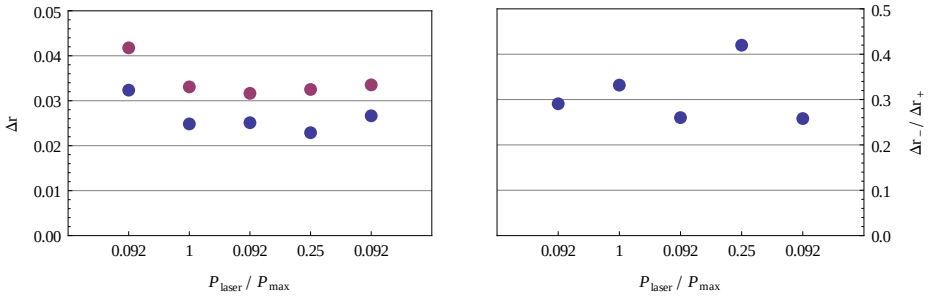

Figure 9: a) Plot of the changes in the ratio for the given stimuli at each laser power, chronologically ordered. In blue we see the difference between the ratio in 0.05 mM and 0.5 mM serine, which we call Δr_+. In red we see the difference between the ratio in MotM and in 0.5 mM serine, which we call $\Delta r_+ + \Delta r_-$. b) This plot shows the ratio between Δr_- and Δr_+ at each laser power, in chronological order. For these plots, the uncertainty in the data points, as calculated by taking the standard error of the mean, was smaller than the point size.

2.2.2 Timing strategy

When we want to investigate processes that occur on different time scales, it would be useful to be able to vary the rate at which we acquire data. In this way, we could get more data in a shorter window of time, which would increase the signal-to-noise ratio. This would for instance be useful when we look at the adaptations after addition and removal of attractant.

However, the increased laser exposure might disturb the network. To test this, we performed the following experiment. We used adapting cells, and put them in buffer. Because they adapt, their steady-state kinase activity is close to neither end of the scale, so we are able to see both an attractant and a repellent response. We now exposed the cells to varying sampling frequencies. As a baseline, we took a picture every 10 seconds. We alternated this with higher frame rates of 0.5, 1.5, 2.5 and 5 seconds per frame consecutively.

To analyse the data, we did the following. Firstly, we noted that the effect observed in single cells was of the order of the noise. We therefore decided

to look at the population average. The bleaching correction was done in a different way than for single cells. Namely, we directly fitted a function of the form $A - B_1 \exp(-\lambda_1 x) - B_2 \exp(-\lambda_2 x)$ to the ratio of red to green intensities. Also, we noted that at the end of the measurement, the ratio deviates from this, which we can not explain. We therefore only fitted to the first four periods where the time per frame was 10 s. The result of this can be see in figure 10.

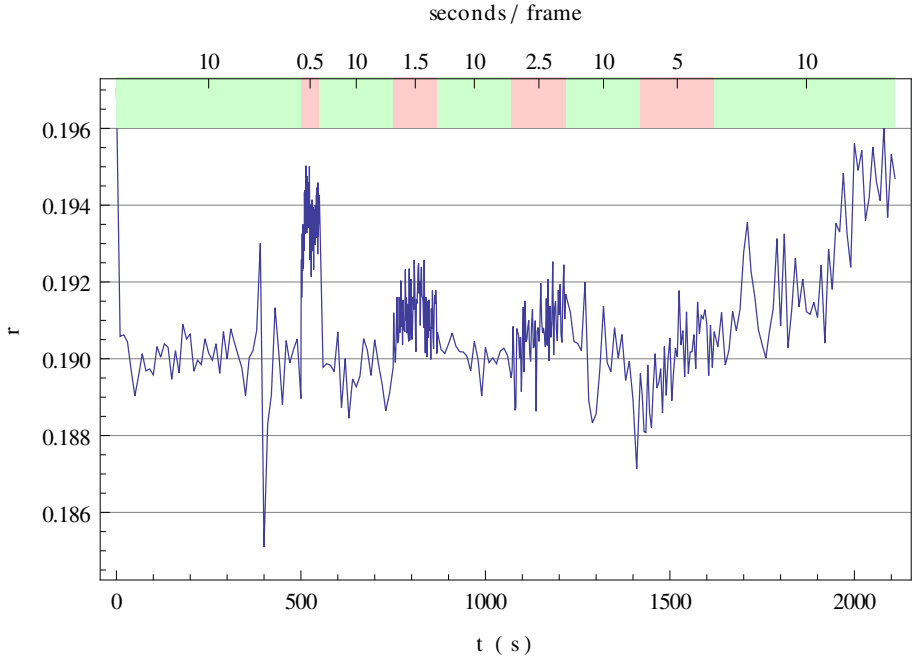

Figure 10: Plot of the FRET ratio in the experiment where we varied the acquisition rate. No chemical stimuli were applied.

We now note, that the ratio changes significantly when the sampling frequency is varied. We therefore conclude that it is not a good idea to use a timing strategy where the sampling rate changes during the measurement. There seems to be not much difference between the timing that we normally use (5 s) and the 10 second one. This is consistent with what we found in the previous section, where we saw that there is no need to lower the laser power. From this experiment we can conclude that it is not wise to increase the laser power, certainly not by more than a factor of 2.

3 Results

In this section, I will describe what we have done to characterize the cell-to-cell variability in *E. coli*'s chemotaxis network.

3.1 Dose-responses of non-adapting cells

Our first application of the single-cell FRET technique was in determining the response of individual *E. coli* cells to serine. This was done in a non-adapting strain. This means, that the cells did not express CheR and CheB. Therefore, the methylation of the kinase/receptor is assumed to be constant. Because the cells do not adapt to their environment, we can give multiple consecutive stimuli without worry that the system components will change.

We gave the cells different step stimuli, from very small to saturating concentrations of L-serine. Before each stimulus, we had the cells in MotM. The cells were exposed to each stimulus for one minute, after which the stimulus was removed. After another minute, the new stimulus was applied. In this way, we get a baseline value for the kinase activity as the value of a when the cells are emerged in MotM. This value is assumed to be close to 1 for this strain. We also get a value for a for each concentration of L-serine that we apply.

The measurements were split into two parts. During the first half of the measurement, we increased the stimulus size from zero to saturation. This we call the forward protocol. After this we decreased the size of the step stimuli, we call this the reverse protocol.

3.1.1 Data for a single cell

When the cells are exposed to the protocol as noted above, their kinase activities will indeed change, as evidenced by the ratio of the light intensities measured in the green and in the red channel. According to equations 5 and 6, the change in the ratio is proportional to the kinase activity. For each cell, we rescale to $a \in [0, 1]$, where $a = 1$ is defined as r_0, the ratio in MotM, and $a = 0$ as the ratio in a saturating stimulus. The difference in FRET between $a = 0$ and $a = 1$ we call F, this is the maximal stimulus size for a given cell.

Now we can fit the Hill function 3 to the data. This leads to parameters $k_{\frac{1}{2}}$ and H for each cell.

This process gives us results like the one illustrated in figure 11.

3.1.2 Selection criteria

Now we would like to look at the distribution of the parameters that signify the response, which are $k_{\frac{1}{2}}$ and H. However, the signal quality varies greatly from cell to cell. When we look at the distribution, we therefore investigate also how strict we should be in selecting the data.

We first note that with our experimental strategy, it is only possible to find values for $k_{\frac{1}{2}}$ that are somewhere between roughly 0.01 and 0.1 mM. This is due

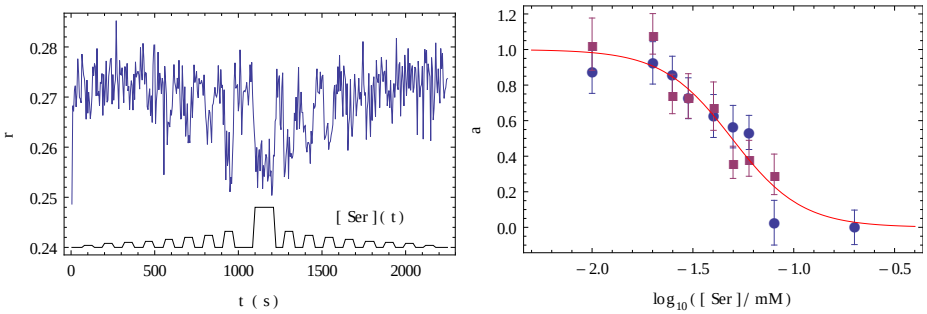

(a) (b)

Figure 11: a) Typical ratio signal for one non-adapting cell in blue. Also indicated is the applied serine concentration, ranging from 0 to 0.20 mM. b) Dose-response curve for this cell. The blue points are the data points for the forward protocol, the purple are for the removal protocol (see section 3.1.5). The red curve is the fitted Hill function. This fit gives $k_{\frac{1}{2}} = 0.049 \pm 0.003$ mM, $H = 2.5 \pm 0.4$. The maximal FRET response is $F = 0.026 \pm 0.002$.

to the fact that we have used a saturating concentration of 0.2 mM on day 1 and of 0.5 mM on day 2. In both cases, the next greatest concentration was 0.08 mM. It is therefore not possible to see a dose response curve with the halfway point this high, as there are not enough data points in this region. The same kind of argument applies to the low side of the curve: our smallest stimulus was 0.01mM. If we do find such a value for $k_{\frac{1}{2}}$, we regard this as an artefact. For instance, the cell may not have responded at all. Then the analysis software tries to fit a Hill curve to plain noise, which might result in any nonsense. Therefore, we only look at those cells for which the fitted value of $k_{\frac{1}{2}}$ lies between 0.01 and 0.1 mM.

It is also not possible to find too large values for H, as the resolution in $[L]$ is only 0.01 mM. When we take the derivative of formula 3 at $[L] = k_{\frac{1}{2}}$, we find it to be $-\frac{H}{4k_{\frac{1}{2}}}$. As we cannot observe derivatives of $a \in [0, 1]$ larger than $\frac{1}{0.01mM}$, we cannot find reliable fits if $H > 400k_{\frac{1}{2}}/mM$, so we take this as an additional criterion.

We have also investigated if the distributions depend on the quality of the fits. To do this, we selected cells for which the relative error in the fit parameters met certain criteria. The mean and standard deviation of the distribution did not depend on the strictness of our criteria. Because of this, we decided to use all cells for which the relative error in the fit parameters was less than 1.

3.1.3 Dose-response parameters

Now we are ready to investigate how the cell-to-cell variation in the DRC's looks like. When we select our cells as described in the previous section, we

end up with 120 bacteria from four different batches, two for each measurement day. We fitted Hill curves to the data of the forward protocol. This resulted in distributions for $k_{\frac{1}{2}}$, H and F as in figures 12a, 12b and 12c. When determining $k_{\frac{1}{2}}$ and H, a subtlety arises due to the usage of only the forward protocol. This is described in paragraph 3.1.5. It forces us to dismiss 9 additional cells, hence we have only data for 111 bacteria.

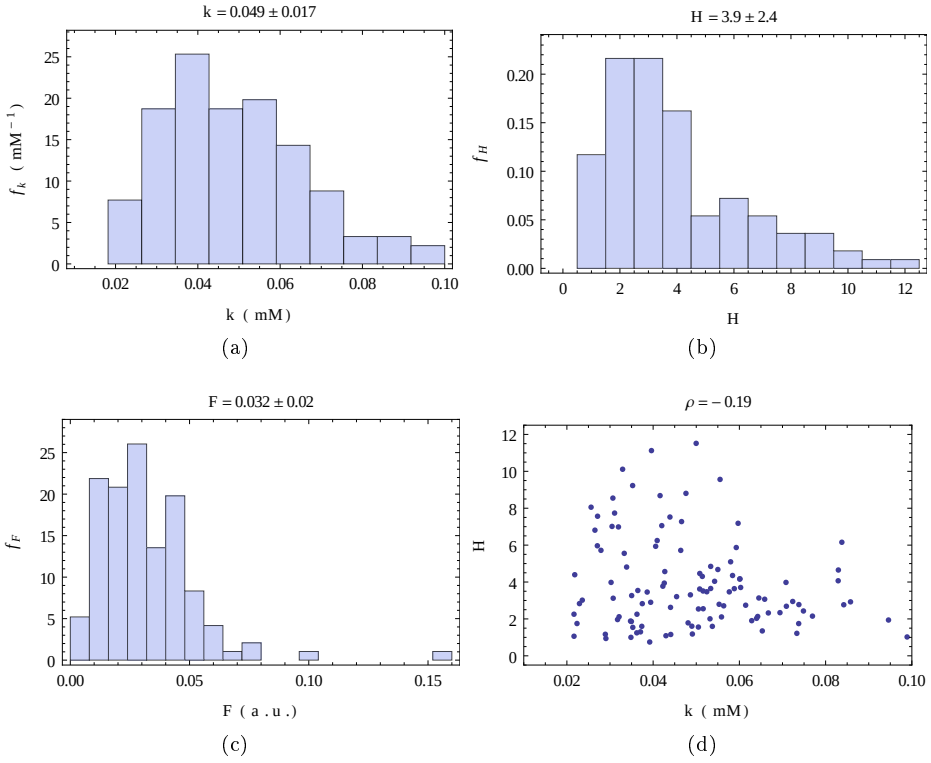

Figure 12: a)-c) Histograms showing the probability density of dose-response parameters over 111 non-adapting cells. a) for $k_{\frac{1}{2}}$ (mM). b) for H. c) for F. d) Plot showing the amount of correlation between $k_{\frac{1}{2}}$ (mM) and H in 111 non-adapting cells.

Now that we have found distributions of parameters, we might investigate if there is any correlation between them, especially for the response parameters $k_{\frac{1}{2}}$ and H. This was done in figure 12d. We find a correlation coefficient of $\rho = -0.19$, which is significant at a significance level of 0.05. However, there is an experimental explanation for this negative correlation. We see that there are no combinations $(k_{\frac{1}{2}}, H)$ where they are both large. This is due to the fact, that we did not take any measurements at serine concentrations higher than 0.08 mM (apart from the saturation). If a cell would have a high Hill coefficient combined

with a high $k_{\frac{1}{2}}$, that would mean that almost all measured kinase activities for this cell would be close to 1 except for the saturating one. This cannot be well fitted. Because of this, we conclude that we do not see enough evidence to say that the correlation between $k_{\frac{1}{2}}$ and H is a property of the system.

3.1.4 Simulated variation

One can wonder if the observed variation in the dose-response parameters is really due to intercellular variability, or that our fitting protocol might induce variations. To test this, we first need to know the uncertainty in our data points. For the uncertainty as determined by standard error-propagation (see appendix A.1), we calculated the mean of the measured uncertainties in the kinase activity for each cell. Then we made a histogram of this, which can be seen in figure 13a.

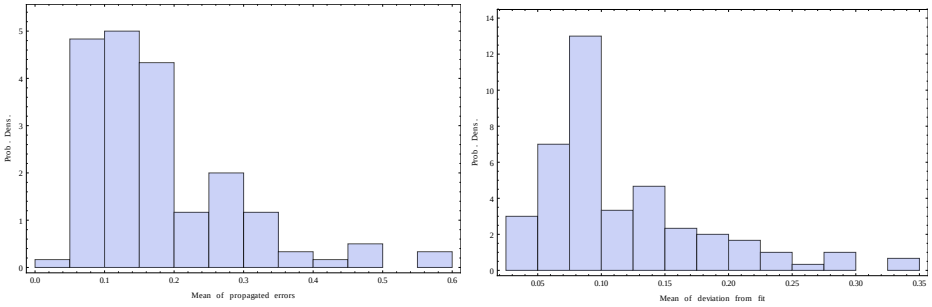

(a) (b)

Figure 13: Histograms of, for each cell, the mean of a) the propagated errors in the kinase activity. b) the deviation from the fit.

As this might not reflect the actual uncertainty in the fitting, for each data point we calculated the difference between the measured value and the fit. Of this difference we took the mean for each cell. A histogram of the result of this is shown in figure 13b. We see that for about half of the cells, the kinase activity is determined within 10% on average.

Now we performed the following simulation. We generated kinase activity data sets from a Hill curve with $k_{\frac{1}{2}} = 0.049$ and $H = 3.9$, at the concentrations we used for the measurement, given fixed values of the standard deviation σ in a. We looked at $\sigma = 0.1$ and $\sigma = 0.2$. We then fitted Hill curves like we did for the measured data. Here we selected according to the same criteria as for the measured data. This gives histograms of the DRC parameters like in figure 14. In table 1 we have summarised the mean and standard deviation of these histograms. We simulated 1000 cells.

As we can see, the broadness of the simulated histogram for H is of comparable magnitude as the broadness of the measured histogram. The same cannot be said for the $k_{\frac{1}{2}}$-histogram: even at a tolerant $\sigma = 0.2$, the simulated histogram

is markedly narrower than the measured one.

We also notice that the average Hill coefficient found is much bigger than the specified $H = 3.9$. This is due to the fact that a negative Hill coefficient is non-physical, so the distribution is tailed to the right.

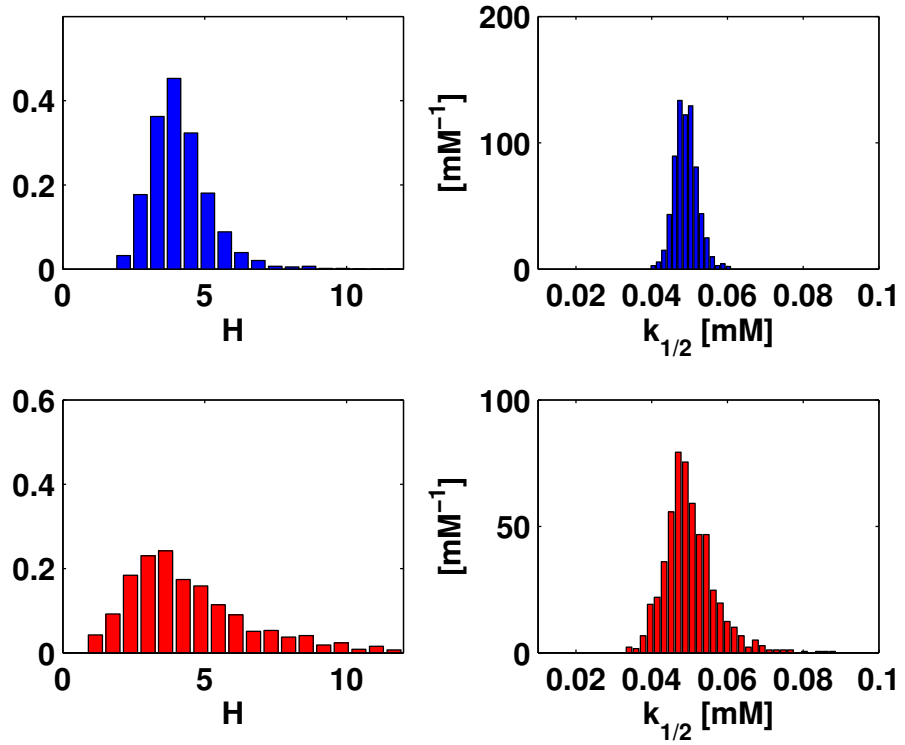

Figure 14: Simulated probability density functions for H (left) and $k_{\frac{1}{2}}$ (right), for an uncertainty σ in the measurements of 0.1 (blue) and 0.2 (red).

	$< H > \pm \sigma H$	$< k_{\frac{1}{2}} > \pm \sigma_{k_{\frac{1}{2}}}$ (mM)
$\sigma = 0.1$	4.1 ± 1.1	0.049 ± 0.003
$\sigma = 0.2$	4.8 ± 2.9	0.050 ± 0.007

Table 1: Overview of the found dose-response parameters in the simulation from figure 14.

To get more insight in how the broadness of the found histograms depends on σ, we now repeated the simulation for different values of σ. The result of this is shown in figure 15. We see that the wideness of the simulated distributions does not increase too much when $\sigma > 0.2$. We do see that the fit procedure

begins to fail sometimes when $\sigma = 0.15$, and that we need to apply our selection criteria quite often for $\sigma > 0.2$.

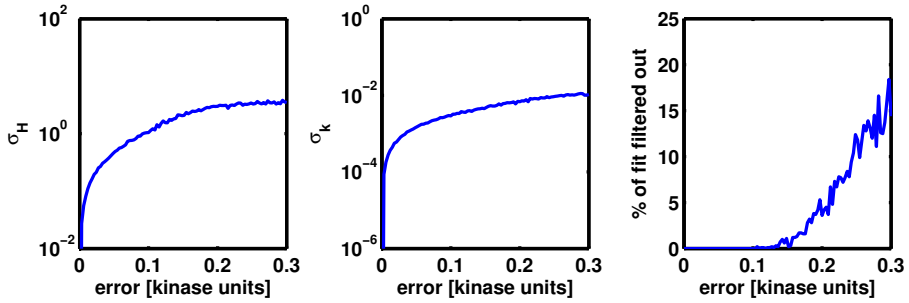

Figure 15: Left: standard deviation of simulated probability density for H as a function of σ. Middle: standard deviation of simulated probability density for $k_{\frac{1}{2}}$ as a function of σ. Right: percentage of simulated data sets that was filtered out by our selection criteria.

From this analysis we conclude that the variation that we observe in the Hill coefficient can be mostly attributed to the fitting procedure, as the standard deviations of the measured and the simulated distributions are comparable. However, the variability in $k_{\frac{1}{2}}$ in our data is much larger than the variability in the simulation. This leads us to conclude that the variability that we observe in this parameter is really due to cell-to-cell heterogeneity.

3.1.5 Increasing and decreasing stimulus size

To check whether our stimuli change the cells in some way, we split up the experiment in a forward and a reverse protocol. During the forward protocol, we kept increasing the stimulus size until saturation. After this, we applied the same stimuli in reverse order until they were decreased to the starting point.

On the first day of experimenting, we used 0.2 mM of L-serine as our maximum stimulus. As a preliminary analysis showed that this concentration might be slightly too low to saturate all cells, we used a maximum $[Ser]$ of 0.5 mM on the second day.

When we compare the kinase activities in the forward protocol with those in the reverse protocol, we see that a appears to be higher in the reverse protocol. This was especially pronounced in the data with $[Ser]_{max} = 0.5$ mM. To check this, we fitted a Hill curve to both the forward and reverse data sets individually. This resulted in the following: the average $k_{\frac{1}{2}}$ of the forward protocol is lower than that of the reverse protocol. This agrees with our findings about the ratios between kinase activities. In the Hill coefficient we do not see much difference. However, an important point now rises: when we fit a Hill curve to both data sets combined, we will find a $k_{\frac{1}{2}}$ that lies somewhere in the middle, but the Hill coefficient will be lower. This is illustrated in figure 16.

Hence, when we analysed the distributions of dose-response parameters in section 3.1.3, we did not consider the reverse protocol.

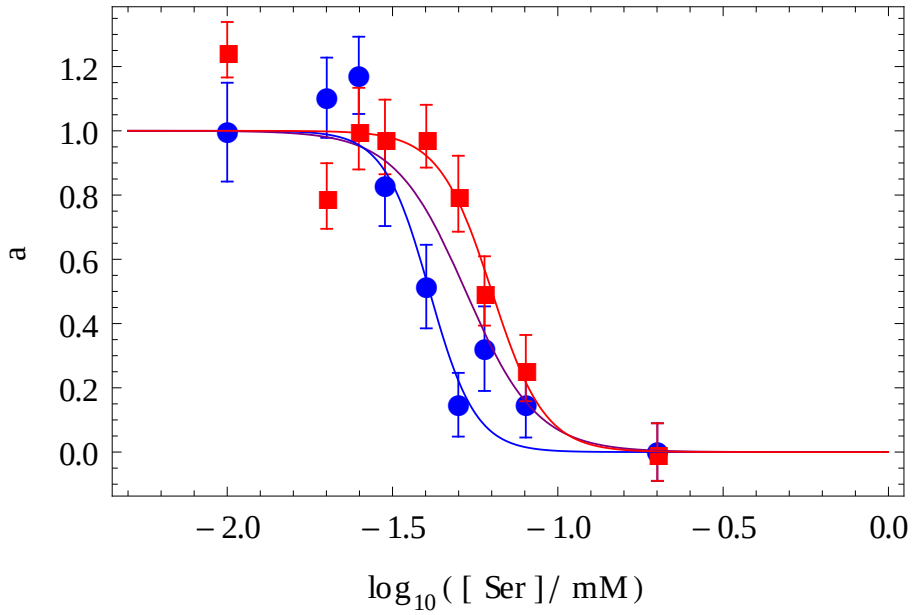

Figure 16: Data and fits for the forward and reverse protocols. In blue we see the forward protocol, in red the reverse. The purple fit uses all data points.

data used for fit	forward	reverse	both
$k_{\frac{1}{2}}$ (mM)	0.041 ± 0.003	0.063 ± 0.005	0.053 ± 0.004
H	6.2 ± 2.3	5.4 ± 2.2	4.0 ± 1.4

Figure 17: Dose-response parameters for this cell with fits using only data from the forward protocol, only from the reverse protocol, and both.

We have also used the two protocols to analyse how our signal quality evolves over time. For each stimulus size, we did the following. We calculated the signal-to-noise ratio $STNR = \frac{a}{\sigma_a}$ for each cell. We then compared the STNR for the forward and reverse protocol by taking the ratio $\frac{STNR_1}{STNR_2}$ where $STNR_1$ is the signal-to-noise ratio as measured in the forward protocol for a given stimulus and $STNR_2$ that in the reverse protocol. We now calculated the distributions of this ratio. The means and standard deviations of those distributions are illustrated in figure 18.

This measurement was done twice, with slightly different conditions. On day 1 the highest serine concentration that we applied was 0.2 mM, on day 2 it was 0.5 mM. The other concentrations were identical. Furthermore, on day 1

the time between the forward and reverse protocols was 2 minutes longer than on day 2, because we applied the saturating concentration for a longer time.

When we look at the data, we notice three things. Firstly, the ratio of the signal-to-noise ratios is pretty constant throughout the measurement. Note that the time between the applications of the smallest stimulus was much longer than the time between the applications of the largest non-saturating stimulus. This indicates that our signal quality remains approximately constant over time. Because the intensity signals are much larger than zero throughout the measurement, the ratio of red to green intensity remains well-determined. This is encouraging if we want to extend the measurements to longer durations.

Secondly, we see that the standard deviation is larger for higher concentrations. This is easily explained: when the concentration is high, the kinase activity approaches zero for many cells. Then the signal-to-noise ratio $STNR_2$ goes to zero, hence the ratio of STNR's diverges.

Finally, we see that the ratio of signal-to-noise ratios is smaller than 1. This effect is strongest in the data of the second day. What this means, is that the signal-to-noise ratio is larger for the reverse protocol. However, we did not change the acquisition method with the protocol, so the only variable in time is photobleaching. But decreasing intensities mean more fluctuations in the FRET ratio, so we would expect that photobleaching decreases the signal quality. As there is no apparent experimental reason why the signal quality is higher in the reverse protocol, we suspect that it might be a property of the chemotaxis network.

3.1.6 Discussion

From the found distribution for $k_{\frac{1}{2}}$, it is clear that there is variability between cells. We also discovered that the $k_{\frac{1}{2}}$ may be changing during the measurement. As was stated in equations 4, $k_{\frac{1}{2}}$ depends on two things: the dissociation constant K_I of ligand for inactive receptors and the free energy $f_m(m)$ due to the methylation state of the receptor. As we are working with cells that do not express CheR and CheB, the methylation level of the receptors is assumed to be constant, for all receptors are created in the same way and there are no enzymes to methylate or demethylate. This makes us think that the value of K_I might be different from cell to cell. Maybe it can even change when stimuli are applied.

As was shown in a recent paper[2], application of a stimulus can alter the way in which the receptors are clustered. We can imagine that this can have an influence on K_I, as the receptors will change shape due to their interactions. When the shape of a receptor changes, its affinity for ligand also changes.

We have also seen that our signal quality does not change in time, but it might increase after applying large stimuli. In [3], we can read that the signalling network causes non-stimulated cells to exhibit behavioural fluctuations on much larger time scales than statistically expected. This indicates that a large part of the noise in the measured kinase activity might actually be due to noise in the cells, as opposed to noise from the measurement apparatus. If the signalling

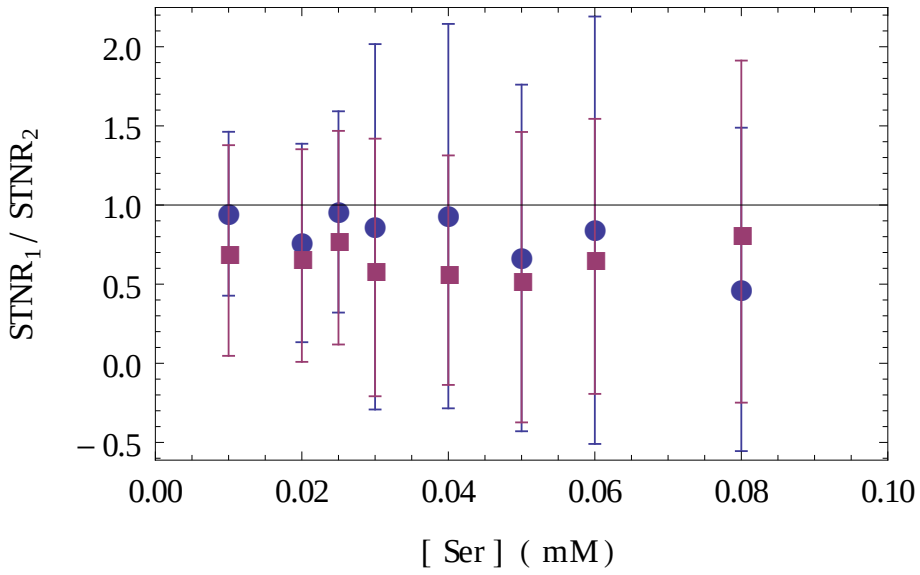

Figure 18: Plot of the ratio of the signal-to-noise ratios measured at different serine concentrations in the forward and reverse protocol. The blue squares give the data for the first measurement day, the red squares for the second. The non-saturating concentrations that we used did not vary between the days. On day 1 we used a highest concentration of 0.2 mM L-serine, on day 2 of 0.5 mM. Error bars signify the standard deviation of the measured distributions of the ratio of signal-to-noise ratios.

network is disturbed by the application of a stimulus, this can also influence the temporal noise in the system. The changing signal quality might therefore be explained by the same effect as the variability in $k_{\frac{1}{2}}$.

3.2 Adapting cells

Now we know that we can perform FRET measurements on a single-cell level to get the distributions of response parameters, we would like to apply this technique to cells that are closer to wild-type: adapting cells. These cells do express the proteins CheR and CheB. This means, that they will adapt to their environment by changing the methylation state of the receptors. An important feature of the system is, that a typical *E. coli* cell has only a couple of hundreds of copies of CheR and CheB (as opposed to several thousands for CheY and CheZ). This means, that we expect a lot of variability in the adaptation system between cells.

We would like to do get probability distributions of adaptation parameters on a single-cell level. The first parameter that we are interested in is a_0, the value of the steady-state kinase activity. Also interesting are τ_{Add} and τ_{Rem}, the time it takes the kinase activity to recover to half its original value after the addition or removal of stimulus, respectively.

A problem with the single-cell FRET technique is, that we cannot look at the data in real-time. Hence, we want to find a good protocol using the knowledge of adapting cells. We have performed the experiment as explained in section 1.3.5 with different amounts of attractant, to decide on a good strategy: the used concentration must be large enough to saturate both responses, but as small as possible to minimize the time we have to wait before the attractant adaptation begins. Namely, this time in which the system is at saturation is a drain on our photon budget. We have found that the removal response saturates at a MeAsp concentration of about 0.5 mM, so we decided to use this value. Furthermore, with this protocol, we have found a population average for a_0 of 0.305, which agrees with what is in the literature[9] for a slightly different strain. For graphs of the results, see figure 19.

The experiments on adapting cells were done on one day, on two different cover slips with cells from the same culture.

3.2.1 Overview of the data

When we use this protocol on the single-cell, we get results as in figure 20. As the raw data is very noisy, we take a moving average of it to get insight in the data. As we can see, we are able to acquire data for single cells that show adaptation to both addition and removal of saturating stimulus.

An interesting feature can be seen: the adaptation seems to occur on a quicker time scale than observed in a population. Single cells switch rather quickly from $a = 0$ to $a = a_0$, but the length of time that the bacterium stays at $a = 0$ varies from cell to cell. This causes the population adaptation time scale to be more spread out.

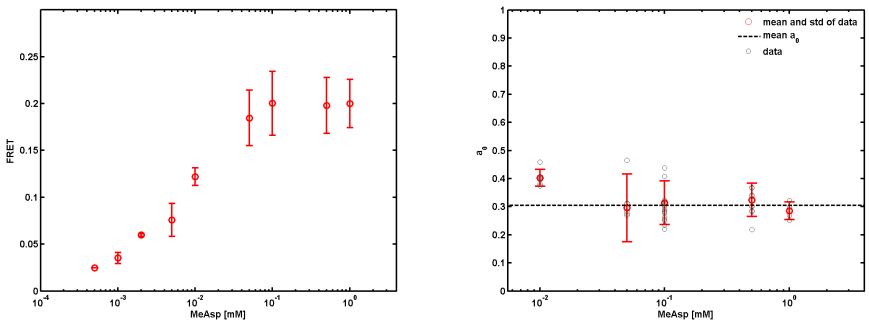

(a) (b)

Figure 19: a) Plot of the total FRET response of a population of adapting cells, as a function of the used concentration of MeAsp. b) Plot of the data acquired to get the mean steady-state kinase activity.

In the following sections I will explain what we have done to extract the steady-state kinase activity and the adaptation time scales from this data.

3.2.2 Steady-state kinase activity

In order to get the steady-state kinase activity for each cell, we need two variables: the maximal change in the ratio and the ratio at steady-state. To get the latter, we take the mean of the red-to-green ratio before addition of stimulus and of that well after the adaptation to the removal of the stimulus. This yields the steady-state ratior_0. For Δr_{max}, the maximal change in ratio, we need the ratio where $a = 0$, which is attained directly after addition of attractant, and the ratio where $a = 1$, which is attained directly after the removal of attractant (provided that the attractant saturates both responses, which we ensured it did). We took the mean of frames 6-20 after addition to get the ratio r_{Add} for $a = 0$ and of frames 3-7 after removal to get the ratio r_{Rem} for $a = 1$.

Now we find $\Delta r_{max} = r_{Rem} - r_{Add}$ and $a_0 = \frac{r_0 - r_{Add}}{\Delta r_{max}}$.

To remove non-physical results, we selected only those cells with $-0.1 < a_0 < 1.1$, 98 cells out of 121 detected ones fulfilled this requirement. We included values slightly below 0 and above 1 as some noise may induce such a seemingly impossible result. We then found a distribution of a_0 as in figure 21a.

Like we did for the non-adapting cells, we also determined the maximal FRET response $F = \frac{\Delta r_{max}}{r_0 + \alpha}$, the distribution that we found is shown in figure 21b. The general shape is similar to the result on non-adapting cells. We do see that the average FRET response in the adapting cells is only about half of what we saw for the non-adapting cells.

We also investigated possible correlations between a_0 and F. As can be seen in figure 22a, we find a negative correlation with a linear correlation coefficient of $\rho = -0.27$. As we had 98 cells, this is significant at a significance level of 0.05.

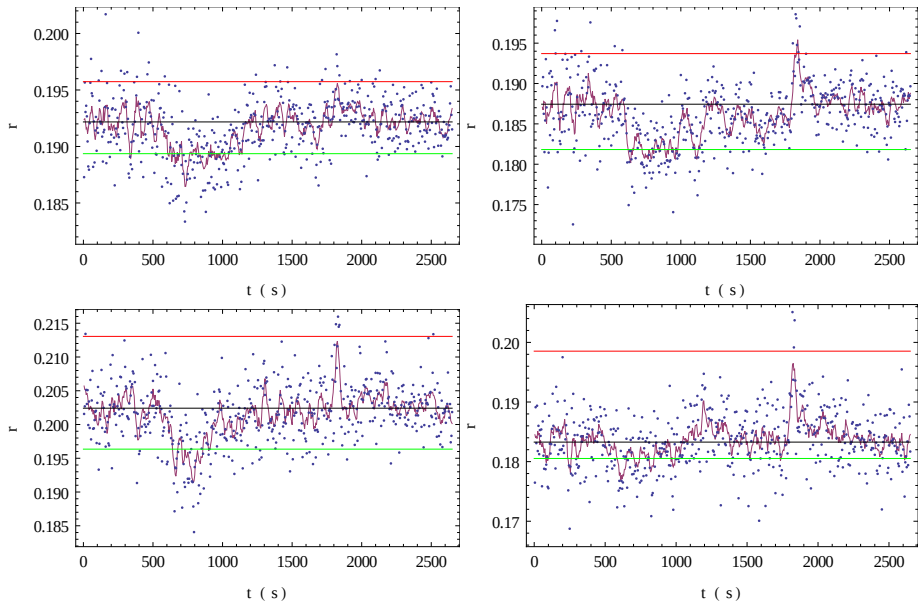

Figure 20: Graphs of the measured ratio for different cells that first adapt to an attractant addition and then to the subsequent removal of that attractant. The blue points give the raw data. The purple line is a moving average of the data, using a window of 7 points. Also indicated are the values for r_0, r_{Add} and r_{Rem} in black, green and red, respectively.

A possible experimental explanation for this might be the following. When a cell has a very small FRET signal, the noise in the data is much larger than the response to stimulus. We can thus determine a_0 less precisely. This means that, for lower F, the distribution for a_0 will get broader. Because the mean of a_0 is closer to 0 than to 1, this effect will be more pronounced towards the high end of the distribution as we throw away negative values for a_0. We could therefore try to select only cells with a high enough FRET response, however this has the drawback that we might throw away too many cells.

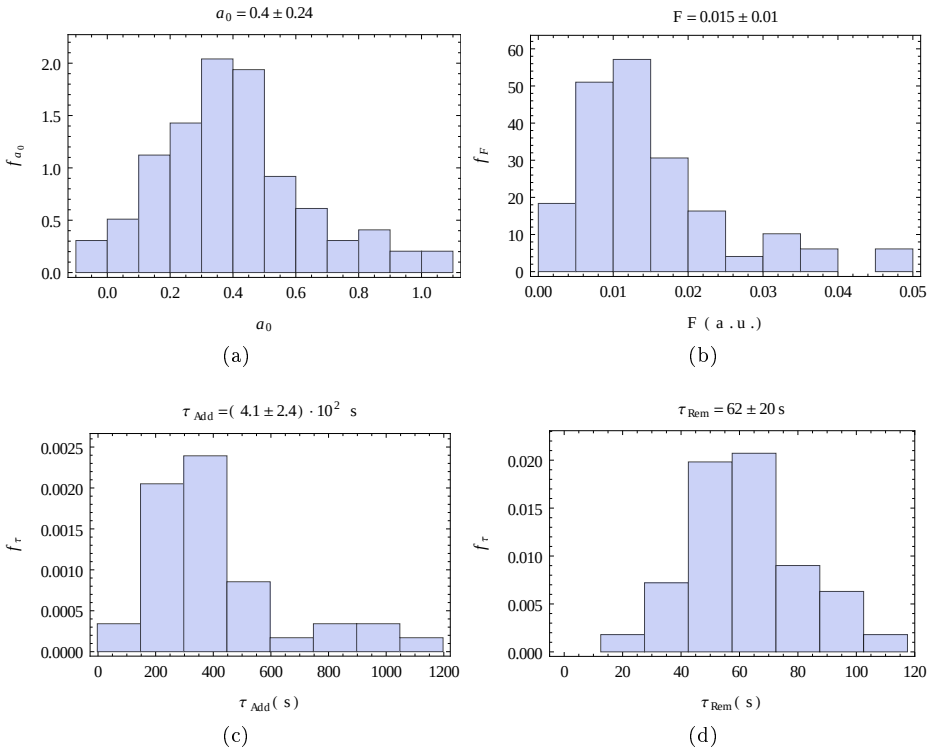

Figure 21: Histograms showing the probability density of a) the steady-state kinase activity of 98 adapting cells. b) the maximal FRET response of 98 adapting cells. c) the addition adaptation time scale of 39 adapting cells. 38 Cells gave Indeterminate, 21 Infinity. d) the removal adaptation time scale of 74 adapting cells. 14 Cells gave Indeterminate, 9 Infinity.

3.2.3 Recovery time

Another interesting parameter of the adaptation, is the time which it takes for a given cell to reach its steady-state. For the addition recovery, we would like to know when the kinase activity recovers to $a = \frac{1}{2}a_0$, and for the removal

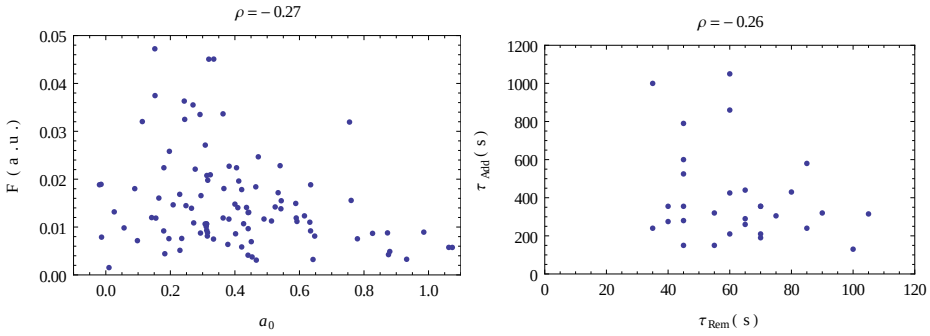

(a) (b)

Figure 22: Plots showing the amount of correlation between a) a_0 and F in 98 adapting cells. b) τ_{Add}(s) and τ_{Rem}(s) in 30 adapting cells.

recovery likewise to $a = \frac{1}{2} + \frac{1}{2}a_0$. To get this, we first applied a moving average to the data as otherwise it is too noisy. If we found no crossings of the values stated, we concluded that the cell had not adapted yet. We associate to this a recovery time of Infinity. If we found multiple crossings, we checked first if the crossings were close together. If they are, we take the mean of the crossings, if not, we conclude that either the data is too noisy or we are dealing with bistable behaviour. In the latter two cases, we do not further consider the data and call the recovery time Indeterminate. We only considered cells for which a_0 could be determined.

Typically, the addition adaptation takes a longer time and is noisier, because, as we have seen, the steady-state kinase activity is usually below $\frac{1}{2}$. Therefore, we analysed both adaptations in a different way. To find the addition adaptation τ_{Add}, we took a moving average with a window of 41 data points. For the removal adaptation time τ_{Rem}, we took 5 data points. Also, we took the mean of the crossings if they were all within 10 frames for the addition and within 4 frames for the removal. Note here that 1 frame corresponds to 5 seconds. The total length in which we checked the addition adaptation was 1200 seconds, for the removal adaptation this was 120 s.

The distribution that we found for the addition response can be found in figure 21c. We found 39 cells of which we could determine τ_{Add}, 21 had not adapted before we removed the attractant and for 38 cells, it was not possible to find a value for τ_{Add} in the manner described. A similar distribution was found for τ_{Rem}, see figure 21d. We succeeded in finding τ_{Rem} for 74 cells. Now we had 9 cells which had not yet adapted and 14 cells for which we could not determine the removal adaptation time.

Because CheR and CheB are expressed from the same operon, we expect that there is a positive correlation between the concentrations of CheR and CheB in the cell. As more CheR means more methylation so a faster adaptation to addition of attractant, and more CheB means more demethylation so a faster

adaptation to removal of attractant, we expect a positive correlation between τ_{Add} and τ_{Rem}. To check this hypothesis, we made a scatter plot. The result of this is shown in figure 22b. Surprisingly, we do not see a significant correlation and what we see, is of opposite sign. We could determine both τ_{Add} and τ_{Rem} for only 30 cells. To be more confident on this issue, we thus need more cells for which both recovery times can be determined.

4 Conclusion

This research has shown that one can use Förster Resonance Energy Transfer to probe the chemotaxis network of Escherichia coli at a single-cell level. We have developed methods to deal with photobleaching and characterized the toxic effect of the laser light.

We have applied FRET first to non-adapting cells. We have shown that there is a significant intercellular variability: $k_{\frac{1}{2}}$ differs from one cell to another. We could not establish significant variability in the Hill coefficient. Also, we could not say unequivocally if these parameters are correlated.

Secondly, we have used FRET to characterize the adaptation characteristics of adapting cells. As we have shown that we can use FRET on adapting cells, a natural continuation of this research would be to acquire dose-response curves also in adapting cells, and look at how the dose-response parameters correlate with the adaptation parameters.

Now that we see variability between single cells, we can ask if we can see this variability also in the cell structure. In our group, François Anquez, Johannes Keegstra and Jacopo Solari are working on techniques with which they can use single-molecule imaging to probe the cellular interior. It will be very interesting to combine the single-cell FRET techniques with their work. This will allow us to correlate the network parameters with information about the physiology of the cells, such as the distribution of receptor clusters.

Another interesting question is how to relate molecular noise to temporal variability on a single-cell level. As previously mentioned, the signalling network has been shown to influence temporal variability on a behavioural level. It would be interesting to see single-cell FRET applied to this: we can monitor the state of the chemotaxis network during the stochastic processes inside the cell.

5 Acknowledgements

The research described in this bachelor's thesis was performed at FOM Institute AMOLF, during an internship beginning September 2012 and ending June 2013. One purpose of the research was to enable me to obtain my degree at Utrecht University. It also served as a final project for the honours programme in experimental physics that I followed during the last two years of my studies.

My work in this project has been the following. I have performed the experiments that were described in sections 2 and 3, with the exception of the population experiments that led to figure 19. I also wrote the analysis code that computed all the results on single cells, taking as input the raw intensity signal for each cell.

During the project I was ably supervised by Tom Shimizu as part of his group Systems Biology. I collaborated intensively with François Anquez and, from January 2013 onwards, with Johannes Keegstra. I was helped in the lab by Simone Boskamp and Milena Lazova. I want to thank them for their guidance, kindness and enthusiasm that made this project such a wonderful experience.

References

[1] Pieter F. de Haan. Chemotaxis in Escherichia coli: studying cell-to-cell variation in response to identical stimuli using FRET. Bachelor's thesis, Utrecht University, 2012.

[2] Vered Frank and Ady Vaknin. Prolonged stimuli alter the bacterial chemosensory clusters. *Molecular Microbiology*, 88:634–644, 2013.

[3] Ekaterina Korobkova, Thierry Emonet, Jose M. G. Vilar, Thomas S. Shimizu, and Philippe Cluzel. From molecular noise to behavioural variability in a single bacterium. *Nature*, 428:574–578, 2004.

[4] Mingshan Li and Gerald L. Hazelbauer. Cellular stoichiometry of the components of the chemotaxis signaling complex. *Journal of Bacteriology*, 186:3687–3694, 2004.

[5] Jacques Monod, Jeffries Wyman, and Jean-Pierre Changeux. On the nature of allosteric transitions: A plausible model. *Journal of Molecular Biology*, 12:88–118, 1965.

[6] Rob Phillips, Jane Kondev, and Julie Theriot. *Physical Biology of the Cell.* Garland Science, 2009.

[7] Thomas S. Shimizu, Yuhai Tu, and Howard C. Berg. A modular gradient-sensing network for chemotaxis in Escherichia coli revealed by responses to time-varying stimuli. *Molecular Systems Biology*, 6:382, 2010.

[8] Victor Sourjik. Receptor clustering and signal processing in E. coli chemotaxis. *Trends in Microbiology*, 12:569–576, 2004.

[9] Victor Sourjik and Howard C. Berg. Receptor sensitivity in bacterial chemotaxis. *PNAS*, 99:123–127, 2002.

[10] Victor Sourjik, Ady Vaknin, Thomas S. Shimizu, and Howard C. Berg. In vivo measurement by FRET of pathway activity in bacterial chemotaxis. *Methods in Enzymology*, 423:365–391, 2007.

[11] Barry L. Taylor and D. E. Koshland, Jr. Intrinsic and extrinsic light response of Salmonella typhimurium and Escherichia coli. *Journal of Bacteriology*, 123:557–569, 1975.

[12] Yuhai Tu, Thomas S. Shimizu, and Howard C. Berg. Modeling the chemotactic response of Escherichia coli to time-varying stimuli. *PNAS*, 105:14855–14860, 2008.

A Appendix

A.1 Error propagation

For the kinase activity a at some stimulus, $a = \frac{F}{F_{max}}$ where F is the FRET signal and F_{max} is the maximum FRET response. Let σ_x denote the uncertainty in variable x. Then $\sigma_a = \frac{\sigma_F}{F_{max}}$.

Now we know $F = \frac{\Delta r}{\alpha + r_0 + \Delta r}$ where r_0 is the FRET ratio at saturating stimulus and Δr is the difference between the measured FRET ratio and r_0. α is a constant, for which we use $\alpha = 0.3$. Then

$$\begin{aligned}
\sigma_F &= \sqrt{\left(\frac{\partial F}{\partial(\Delta r)}\sigma_{\Delta r}\right)^2 + \left(\frac{\partial F}{\partial r_0}\sigma_{r_0}\right)^2} \\
&= \sqrt{\left(\frac{\alpha + r_0 + \Delta r - \Delta r}{(\alpha + r_0 + \Delta r)^2}\sigma_{\Delta r}\right)^2 + \left(\frac{-\Delta r}{(\alpha + r_0 + \Delta r)^2}\sigma_{r_0}\right)^2} \\
&= \frac{1}{(\alpha + r_0 + \Delta r)^2}\sqrt{(\alpha + r_0)^2\sigma_{\Delta r}^2 + (\Delta r)^2\sigma_{r_0}^2}
\end{aligned}$$

Here $\Delta r = r - r_0$ for r the measured ratio, so $\sigma_{\Delta r} = \sqrt{\sigma_r^2 + \sigma_{r_0}^2}$.

A.2 Strains and plasmids

Three different strains of *Escherichia coli* were used in this experiment.

- For measuring the background fluorescence, we used strain TSS682, which is HCB33, wild-type for chemotaxis, transformed with an empty pTRC99 (Amp resistance/IPTG promotor) and pBAD33 (Cam/Arabinose) plasmids.
- As our adapting cells, we used TSS966 [RB+], a derivative of VS104, which is wildtype with CheY and CheZ deleted. This strain was transformed with a plasmid with a FRET pair expressed in tandem (CheY-mRFP1 / CheZ-YFP on a pTRC99A plasmid) and an empty pBAD33.
- Our non-adapting cells were TSS919 [RB-] is VS149, which is wildtype with CheB, CheR, CheY and CheZ deleted. This strain was transformed with the same plasmids as TSS966.

A.3 Protocols

A.3.1 Growing cells

Stocks of the cells are kept in a -80 °C freezer. From these stocks, we make overnight cultures. These consist of the cells, with appropriate antibiotics to which our cells are resistant: 100 μg/ml ampicilline (Amp) and 34 μg/ml chloramphenicol (Cam), dissolved in TB. This culture is left to saturate overnight

for about 12-16 hours at a temperature of 30 °C. From the overnight culture we then make a day culture, which is almost the same as the overnight culture, but in addition also contains an inducer, IPTG at a concentration of 10 μM. The day culture is left in an incubator to grow for 4-5 hours at 33.5 °C. Near the end of growth, we measure the optical density (OD) in a spectroscope at 600 nm. When the OD is between 0.45 and 0.47, we take the cells out of the incubator.

Now the cells are spun down in a centrifuge for 5 minutes at 5000 rpm. We then throw away the TB medium and dissolve the cells in MotM at the same density as in the TB. We centrifuge three times in total, in order to fully replenish the medium. This stops the growth of the cells. When changing the medium, we must be careful to dissolve all of the cells in the new medium. However, no excessive flow, such as pipetting inside, should be used as this destroys the flagella.

Now the cells are put in a 4 °C fridge and left for at least 30 minutes. This is done to get the protein expression levels constant. The bacteria are left in the fridge for at most 5 hours. During this time, we take cells from this solution to measure on. The density is still the same: the cells are dissolved in 10 ml of MotM.

A.3.2 Preparing cover slips

We prepare our samples in the following way. First, we clean both sides of a glass cover slip with pure ethanol and optical paper. We then apply poly-L-lysine on one side for 15-20 minutes. After this, we clean three times with water and three times with MotM. We leave a droplet of MotM resting on the cover slip.

The cover slip will be placed in a flow cell (design: Howard Berg), but not before this is well cleaned with ethanol, water and MotM. It is important to keep the flow cell free of air bubbles. To start without bubbles, we can flow ethanol through the flow cell under high pressure, using a syringe, when there is no cover slip attached. We then attach tubing, being careful not to let a bubble in.

When the cells are ready, we remove the MotM from the cover slip and apply some cells to the cover slip. For single-cell imaging, a dilution to an OD of about 0.05-0.10 is necessary. We leave the cells on for at least 15 minutes, after which we remove the surplus liquid. We then insert the cover slip into the flow cell, using vacuum grease.

The cells are stimulated using solutions of L-serine in MotM for non-adapting cells and of L-methyl-aspartate in MotM for adapting cells.

A.3.3 Data acquisition

When the cells are in the microscopy set-up, we find suitable region of interest under bright-field imaging. When we have found one, we take a bright field picture for reference on the attachment. We put the focus slightly off, such that well-attached cells look darker than their environment. After this we bring the

cells into focus. The cells are then almost indistinguishable from the surroundings.

For our camera settings, we have used a gain of 1, a gain multiplication factor of 100 and a laser power of 30 mW throughout all experiments.

When the camera is not being exposed to light, small amounts of electrical charge build up on the CCD. This induces noise in the signal. The charge is wiped away when the frame is read out. When the sampling frequency is constant, we can set up the camera, so that it takes an unexposed frame shortly before it takes the exposed one. This cleans the CCD directly before it is being exposed instead of several seconds earlier. This reduces some noise.

A.4 Chemicals

A.4.1 Motility medium (MotM)

Final concentrations:

- 10 mM potassium phosphate
- 0.1mM EDTA
- 1 μM methionine
- 10 mM lactic acid
- Adjust to pH=7.0 with saturated NaOH.

Stocks:

- 1M potassium phosphate (by mixing 1M K_2HPO_4 and KH_2PO_4 until pH=7.0) (dilute 100x)
- 100 μM L-methionine (100x)
- 1M lactic acid (100x)
- 10 mM EDTA (100x)

A.4.2 Tryptone broth (TB)

- 10g bacto tryptone (1% final concentration)
- 5g NaCl (0,5% final concentration)
- Fill up to 1l and dissolve the components by stirring and heating.
- Adjust the pH to 7.0
- Autoclave the media